JCIM JOURNAL OF CHEMICAL INFORMATION AND MODELING

Article

Cite This: J. Chem. Inf. Model. 2020, 60, 259−267

pubs.acs.org/jcim

GUI Implementation of VCDtools, A Program to Analyze Computed Vibrational Circular Dichroism Spectra

Mark A. J. Koenis,[†] Olivier Visser,[‡] Lucas Visscher,[¶] Wybren J. Buma,*[,†,§] and Valentin P. Nicu*[,∥]

[†]Van 't Hoff Institute for Molecular Sciences, University of Amsterdam, Science Park 904, 1098 XH Amsterdam, The Netherlands

[‡]Software for Chemisty and Materials, De Boelelaan 1083, 1081 HV Amsterdam, The Netherlands

[¶]Amsterdam Center for Multiscale Modeling, Section Theoretical Chemistry, Faculty of Sciences, Vrije Universiteit Amsterdam, De Boelelaan 1083, 1081 HV Amsterdam, The Netherlands

[§]Institute for Molecules and Materials, FELIX Laboratory, Radboud University, Toernooiveld 7c, 6525 ED Nijmegen, The Netherlands

[∥]Department of Environmental Science, Physics, Physical Education and Sport, Lucian Blaga University of Sibiu, loan Ratiu Street, Number 7-9, 550012 Sibiu, Romania

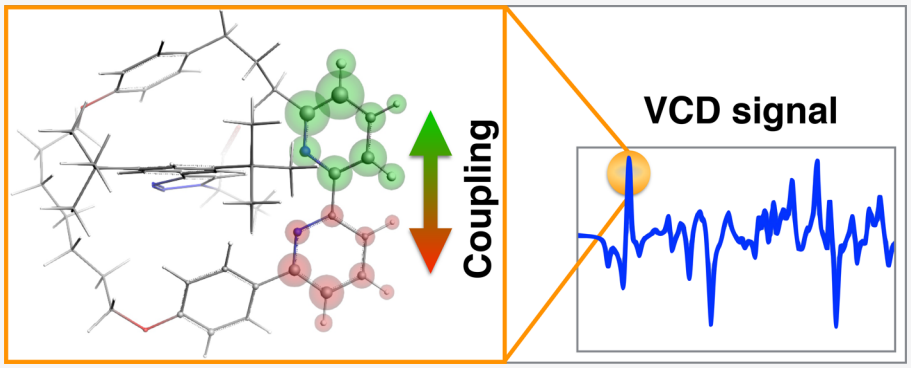

ABSTRACT: As computing power increases, vibrational circular dichroism (VCD) calculations on molecules of larger sizes and complexities become possible. At the same time, the spectra resulting from these computations become increasingly more cumbersome to analyze. Here, we describe the GUI implementation into the Amsterdam Density Functional (ADF) software package of VCDtools, a toolbox that provides a user-friendly means to analyze VCD spectra. Key features are the use of the generalized coupled oscillator analysis methods, as well as an easy visualization of the atomic electric and magnetic transition dipole moments which together provide detailed insight in the origin of the VCD intensity. Using several prototypical examples we demonstrate the functionalities of the program. In particular, we show how the spectra can be analyzed to detect differences between theory and experiment arising from large-amplitude motions or incorrect molecular structures and, most importantly, how the program can be used to prevent incorrect enantiomeric assignments.

INTRODUCTION

Vibrational circular dichroism (VCD) is a spectroscopic technique that probes the difference in absorption of left and right circularly polarized light for vibrational transitions[1−4] and is one of the most accurate techniques to determine the absolute configuration of chiral molecules. As the VCD spectrum is highly sensitive to key details of the molecular structure—much more than commonly used techniques such as IR absorption—it is increasingly also employed to study and determine the structure of complex molecules like enantioselective catalysts,[5,6] bio-organic compounds,[7−10] and supramolecular complexes.[11−17] The interpretation of experimental VCD spectra and the amount of information that can be obtained from these spectra critically depends on the comparison with theoretically predicted spectra.[1−4] To this purpose several groups have put efforts to develop tools to interpret VCD and other vibrational spectroscopy data.[18−21]

Although the computation of such spectra is now relatively straightforward, the high sensitivity of VCD to spatial structure often complicates such a comparison. In fact, it is nowadays recognized that minor changes in structure may have a profound influence on the position, intensity, and sign of predicted VCD bands.[22−29] One of the main complications is the vibrational magnetic dipole transition moment (MDTM), which determines the VCD intensities via a scalar product with the vibrational electric dipole transition moment (EDTM). Unlike the EDTMs, which also determine the IR intensities, the MDTMs are not well understood. Not only are MDTMs 4 orders of magnitude smaller than their electric counterparts, but they are by definition also origin dependent.

Received: October 15, 2019
Published: December 12, 2019

DOI: 10.1021/acs.jcim.9b00956
J. Chem. Inf. Model. 2020, 60, 259−267

To get a better grip on and obtain a more fundamental insight into this sensitivity toward molecular structure, Nicu has introduced a novel approach to analyze computed VCD spectra, the so-called general coupled oscillator (GCO) model.[30] This method is closely related to the standard coupled oscillator (CO) model (also referred to as exciton chirality VCD method), which was introduced in the seventies to interpret VCD signals.[31] Over the years several studies have indicated severe deficits of the CO model,[32−35] and with the introduction of quantum chemical software packages capable of computing accurate VCD spectra,[36−40] the CO model has more or less become obsolete. The GCO method, however, incorporates additional terms that correct for the shortcomings of the CO model and is, therefore, able to decompose the quantum chemically computed VCD signal in an exact manner. This makes the GCO method much more generally applicable.

In the GCO model, which is discussed in more detail afterward, contributions to the VCD signal are decomposed in terms of two fragments **A** and **B**, and the rest of the molecule **R**. Several studies have shown that fragments **A** and **B** can often be chosen such that the GCO term, that is, the contribution to the rotational strength from coupling fragments **A** and **B**, is the dominant term.[28,30,41] Because the GCO contribution contains the coupling between two parts of the structure, it is very sensitive to the relative orientation of these parts. Analyzing computed bands with this model thus intrinsically offers significant advantages as it immediately makes clear toward which aspects of the molecular structure a particular VCD band is sensitive and helps in identifying the underlying reason if one finds that a VCD signal is not calculated correctly.

The GCO VCD analysis was first implemented in the VCDtools program,[42,43] a FORTRAN code that decomposes computed VCD intensities into contributions associated with electrons, nuclei, individual atoms, groups of atoms and molecular orbitals. Here, we report a Graphical User Interface (GUI) implementation of the program in the Amsterdam Density Functional (ADF) software suite.[37] Upon implementing VCDtools, several features have been added to the original program that significantly enhance the user-friendliness of the code and that make it possible to quickly analyze large molecular systems. Main new features include the use of scaling atom sizes to visualize particular VCD properties, allowing for a quick analysis of the origin of the VCD signal. Also, an automated algorithm has been developed that provides a good initial guess for choosing the coupling fragments for any normal mode of interest. In the present article details of the implementation will be presented, and the advantages of the program will be demonstrated using three prototypical examples. These applications provide convincing demonstrations of how discrepancies between computed and experimental spectra can be analyzed using the GCO method. They show how the method allows one to identify the source of the problems and subsequently correct for them. Given the ability of the GCO analysis to identify the source of the problems, assess their severity and subsequently suggest a solution for correcting them, it is clear that it is a major asset for the analysis of VCD spectra and bound to become a standard tool.

GENERAL COUPLED OSCILLATOR ANALYSIS THEORY

In the following a short summary of the general coupled oscillator (GCO) analysis is provided, a full description can be found in ref 30. As already mentioned, the GCO analysis aims at providing physical insight into the underlying VCD mechanisms by decomposing the VCD intensities into contributions that are associated with molecular fragment and with their interaction. The VCD signal is given by

$$\Delta A(j) = A(j)^{LCP} - A(j)^{RCP} = \left(\frac{32\pi^3}{3}\right)\left(\frac{\nu(j)N_A}{hc}\right)R_{01}(j)$$

in which $\nu(j)$ is the frequency of mode j, N_A is Avogadro's constant, and R_{01} is the rotational strength, which is defined as:[44]

$$R_{01}(j) = -\,\mathrm{Im}[\vec{E}_{01}(j)\cdot\vec{M}_{10}(j)] \tag{1}$$

where $\vec{E}_{01}(j)$ is the electric dipole transition moment (EDTM) and $\vec{M}_{10}(j)$ is the magnetic dipole transition moment, while subscripts 0 and 1 indicate a transition from the vibrational ground state to the first excited state. Within the harmonic approximation, the total dipole transition moments (DTMs) $\vec{E}_{01}(j)$ and $\vec{M}_{10}(j)$ are built from their atomic contributions[45]

$$\vec{E}_{01}(j) = \sum_{i=1}^{N}\vec{E}_{01}^{\,i}(j), \qquad \vec{M}_{10}(j) = \sum_{i=1}^{N}\vec{M}_{10}^{\,i}(j) \tag{2}$$

where i runs over all atoms and N is the total number of atoms.

Using eq 2, the total EDTM and MDTM can be decomposed into contributions from various molecular groups that in principle do not necessarily need to consist of atoms that are covalently bound or even close to each other. Defining three fragments within the molecule as fragment **A**, fragment **B**, and the rest of the molecule as fragment **R**, the rotational strength can be split into three contributions

$$\begin{aligned} R_{01}(j) &= -\mathrm{Im}([\vec{E}_{01}^{\,\mathbf{A}}(j) + \vec{E}_{01}^{\,\mathbf{B}}(j) + \vec{E}_{01}^{\,\mathbf{R}}(j)]\cdot \\ &\quad [\vec{M}_{10}^{\,\mathbf{A}}(j) + \vec{M}_{10}^{\,\mathbf{B}}(j) + \vec{M}_{10}^{\,\mathbf{R}}(j)]) \\ &= R_{01}^{\mathbf{GCO}}(j) + R_{01}^{\mathbf{IF}}(j) + R_{01}^{\mathbf{R}}(j) \end{aligned} \tag{3}$$

The first contribution, $R_{01}^{\mathbf{GCO}}(j)$, is what we identify as the GCO contribution and represents the coupling between fragments **A** and **B**

$$R_{01}^{\mathbf{GCO}}(j) = -\mathrm{Im}[\vec{E}_{01}^{\,\mathbf{A}}(j)\cdot\vec{M}_{10}^{\,\mathbf{B}}(j) + \vec{E}_{01}^{\,\mathbf{B}}(j)\cdot\vec{M}_{10}^{\,\mathbf{A}}(j)] \tag{4}$$

where $\vec{E}_{01}^{\,\mathbf{X}}(j)$ and $\vec{M}_{01}^{\,\mathbf{X}}(j)$, with **X** = (**A**, **B**) are the DTMs associated with the two selected fragments. The $R_{01}^{\mathbf{IF}}(j)$ term contains the contribution from the selected individual fragments (IF) **A** and **B**

$$R_{01}^{\mathbf{IF}}(j) = -\mathrm{Im}[\vec{E}_{01}^{\,\mathbf{A}}(j)\cdot\vec{M}_{10}^{\,\mathbf{A}}(j) + \vec{E}_{01}^{\,\mathbf{B}}(j)\cdot\vec{M}_{10}^{\,\mathbf{B}}(j)] \tag{5}$$

The $R_{01}^{\mathbf{R}}(j)$ term contains the VCD intensity deriving from the rest of the molecule and is given by

$$\begin{aligned} R_{01}^{\mathbf{R}}(j) &= -\mathrm{Im}[\vec{E}_{01}^{\,\mathbf{A}}(j)\cdot\vec{M}_{10}^{\,\mathbf{R}}(j) + \vec{E}_{01}^{\,\mathbf{R}}(j)\cdot\vec{M}_{10}^{\,\mathbf{A}}(j) \\ &\quad + \vec{E}_{01}^{\,\mathbf{B}}(j)\cdot\vec{M}_{10}^{\,\mathbf{R}}(j) + \vec{E}_{01}^{\,\mathbf{R}}(j)\cdot\vec{M}_{10}^{\,\mathbf{B}}(j) \\ &\quad + \vec{E}_{01}^{\,\mathbf{R}}(j)\cdot\vec{M}_{10}^{\,\mathbf{R}}(j)] \end{aligned} \tag{6}$$

Since **A** and **B** are the important fragments, the $R_{01}^{\mathbf{GCO}}$ and $R_{01}^{\mathbf{IF}}$ contributions associated with them are expected to account

DOI: 10.1021/acs.jcim.9b00956
J. Chem. Inf. Model. 2020, 60, 259−267

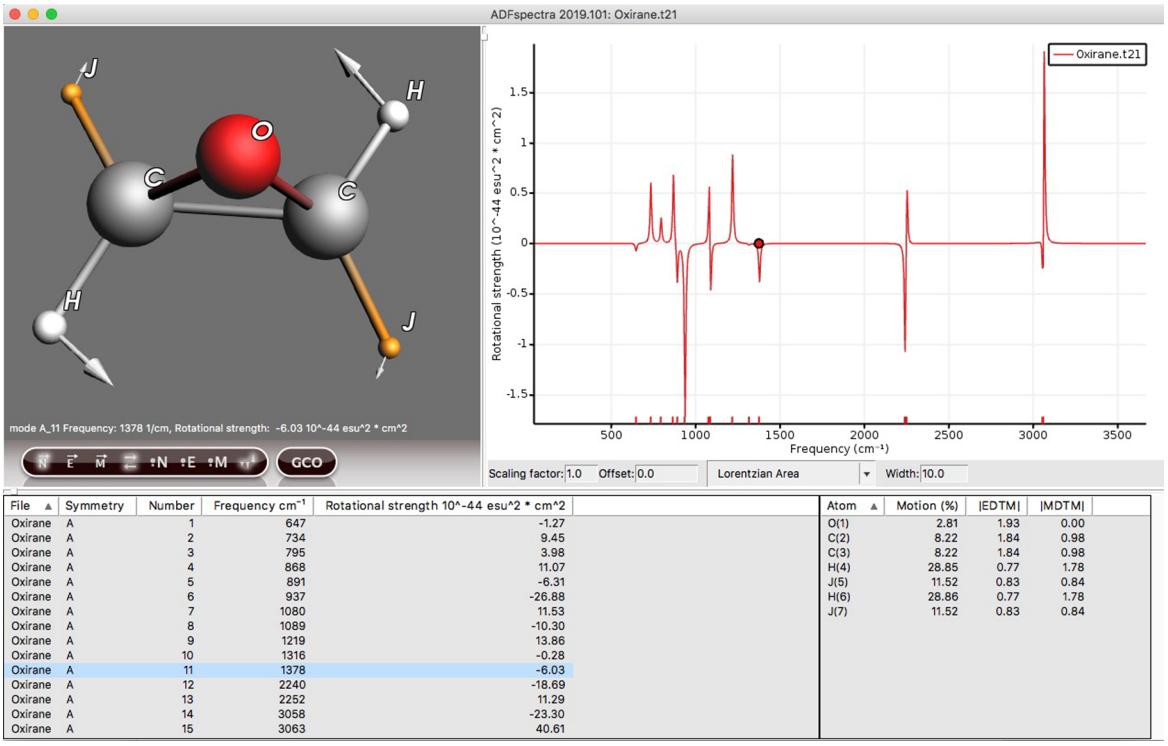

File	Symmetry	Number	Frequency cm^{-1}	Rotational strength 10^-44 esu^2 * cm^2
Oxirane	A	1	647	-1.27
Oxirane	A	2	734	9.45
Oxirane	A	3	795	3.98
Oxirane	A	4	868	11.07
Oxirane	A	5	891	-6.31
Oxirane	A	6	937	-26.88
Oxirane	A	7	1080	11.53
Oxirane	A	8	1089	-10.30
Oxirane	A	9	1219	13.86
Oxirane	A	10	1316	-0.28
Oxirane	A	11	1378	-6.03
Oxirane	A	12	2240	-18.69
Oxirane	A	13	2252	11.29
Oxirane	A	14	3058	-23.30
Oxirane	A	15	3063	40.61

Atom	Motion (%)	|EDTM|	|MDTM|
O(1)	2.81	1.93	0.00
C(2)	8.22	1.84	0.98
C(3)	8.22	1.84	0.98
H(4)	28.85	0.77	1.78
J(5)	11.52	0.83	0.84
H(6)	28.86	0.77	1.78
J(7)	11.52	0.83	0.84

Figure 1. ADFspectra GUI interface showcasing a VCD calculation of partly deuterated oxirane with one of its normal modes selected and shown as white arrows. The deuterium atoms are labeled as "J".

for most of the VCD intensity of a specific normal mode. As has been shown before[30,41] and as will be demonstrated here, $R_{01}^{\mathbf{GCO}}$ is often significantly larger than $R_{01}^{\mathbf{IF}}$, especially when fragments **A** and **B** are achiral. The **R** fragments contain the rest of the atoms and when the GCO fragments are properly chosen, the $R_{01}^{\mathbf{R}}$ contribution is expected to be small. Finally, it should be noticed that the GCO term is closely related to the standard coupled oscillator (CO) model.[31] However, the GCO model is, as its name suggests, more generally applicable as it contains a correction term (COC) to the original CO model,[30] which makes it exact and applicable to all types of normal modes and is given by

$$R_{01}^{\mathbf{GCO}}(j) = R_{01}^{\mathbf{CO}}(j) + R_{01}^{\mathbf{COC}}(j) = \frac{\pi\nu_j}{c}\cdot[\vec{Y}^{\mathbf{CO}} + \vec{Y}^{\mathbf{COC}}]\cdot[\vec{E}_{01}^{\,\mathbf{A}}(j) \times \vec{E}_{01}^{\,\mathbf{B}}(j)] \quad (7)$$

where $R_{01}^{\mathbf{CO}}$ is the standard CO term, $R_{01}^{\mathbf{COC}}$ the coupled oscillator correction term, ν_j the frequency of normal mode j, c the speed of light, $\vec{Y}^{\mathbf{CO}}$ the vector between the center of masses of fragments **A** and **B** and $\vec{Y}^{\mathbf{COC}}$ the through-space vector that corrects for the difference between the CO and GCO model ($\vec{Y}^{\mathbf{GCO}} = \vec{Y}^{\mathbf{CO}} + \vec{Y}^{\mathbf{COC}}$).

VCDTOOLS FEATURES

VCDtools has been embedded into the ADFspectra program, which is part of the ADF software suite.[37,46] This GUI program allows the users to open computed spectra and analyze them. For VCD and vibrational absorption (VA) spectra, it was already possible to select normal modes either in the spectra or from a list and then look at an animation of the mode or show the normal mode vectors on the molecule. In Figure 1, the ADFspectra program is shown displaying the results of a VCD calculation of oxirane. The most frequently used functions of VCDtools are integrated as buttons underneath the molecular structure. Once a normal mode is selected, the atomic contribution to the normal mode, EDTM and MDTM are computed automatically by VCDtools and listed in ADFspectra.

Visualizing Electric and Magnetic Dipole Transition Moments. Even though the normal mode motion induces the atomic EDTMs and MDTMs responsible for the observed VCD bands, the size of the nuclear displacement vectors does not reflect the magnitude of the associated atomic contributions to the VCD signal. It is often the case that the most important atoms for VCD, that is, the ones with the largest contribution to the EDTM and MDTM, have only small or moderate displacements. Take, for example, the normal mode shown in Figure 1, where the C atoms only contribute for 8% to the normal mode but dominantly contribute to the EDTM and MDTM. The underlying reason for this is that movement of these polar bonded C atoms displaces more charge resulting in higher DTMs. This implies that to find the source of the VCD intensity it is much more useful to look at the EDTM instead of the normal mode contribution. Because of its origin dependence, the MDTM is in this respect not as useful.

The implementation of VCDtools gives users several options to display the atomic EDTM and MDTM contributions. They can (i) be printed as text, (ii) shown as vectors in the molecule, or (iii) the atomic spheres can be scaled in size according to their contribution. As we will demonstrate in the application section, the latter option is extremely effective. Especially for large molecules, it is helpful that the parts of the molecule that do not contribute are reduced to a wire frame representation while the important groups are highlighted. The print option is, therefore, mainly useful if exact values need to be known. The vector representation, on the other hand, gives information about the cancellation between different DTMs

DOI: 10.1021/acs.jcim.9b00956
J. Chem. Inf. Model. 2020, 60, 259−267

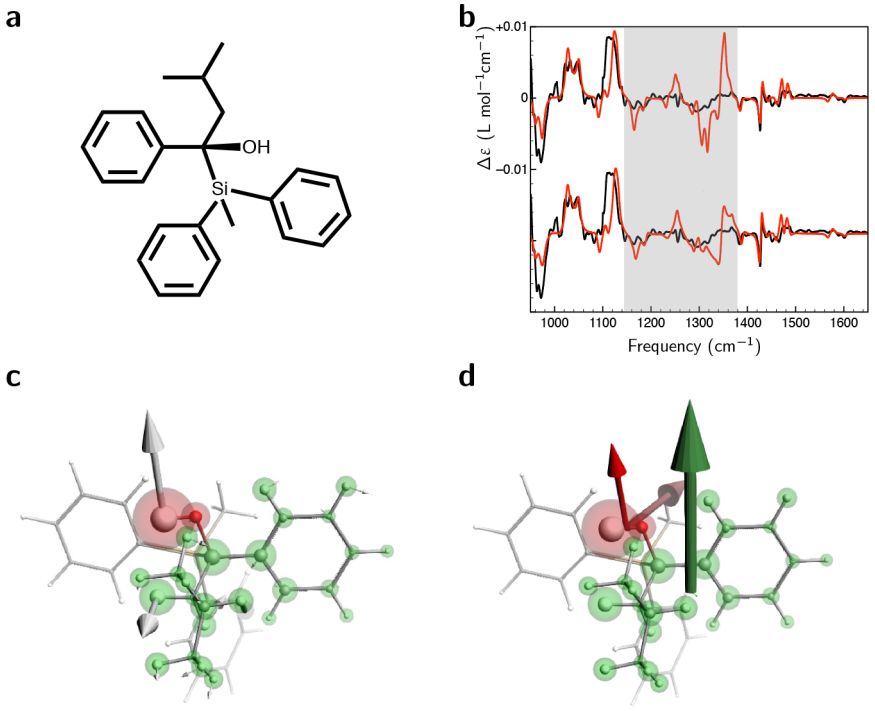

Figure 2. (a) Schematic representation of silyl-alcohol. (b) Experimental (black) and computed VCD spectra (red). The top and bottom computed spectra correspond, respectively, to the normal Boltzmann average and the Boltzmann average when taking the OH bending motion into account using linear transit calculations.[28] Panels c and d display normal mode 107 of the lowest-energy conformer of silyl-alcohol. The atomic spheres are scaled by their atomic EDTMs while the two coupling groups **A** and **B** are highlighted with red and green spheres. Panel c displays the normal mode vectors, and panel d shows the DTM vectors of the selected groups. The dark red and dark green arrows represent the MDTM vectors and the light red and light green arrows the EDTM vectors (the EDTM of the green fragment is very small).

from different parts of the molecule and often provides insightful explanations for why some normal modes give rise to large signals while vibrations that at first sight look similar do not.

General Coupled Oscillator Analysis. An GCO analysis, which computes and prints all contributions, vectors and angles that are relevant to the method (see the previous section), is performed simply by clicking on the "GCO" button (see Figure 1). Such an analysis requires the selection of two molecular fragments, the GCO fragments **A** and **B**. This can easily be done in ADFspectra using the menu *Regions* (ADF nomenclature) which has several options for grouping atoms into fragments and for altering the number of atoms in a fragment. The selected fragments are highlighted in the molecule using transparent spheres in different colors (see Figures 2−4). Once the fragments are selected it is also possible to show the contribution of those regions to the total EDTM and MDTM as arrows placed at the center of each fragment.

For many normal modes defining the molecular fragments is straightforward. One simply scales the atomic spheres with the magnitude of the atomic EDTMs and then assigns the highlighted atoms to the two GCO fragments using physical or chemical intuition. However, when such an identification becomes less obvious VCDtools uses a built-in optimization algorithm that finds and optimizes the coupling fragments. To ensure that the partitioning remains chemically relevant the algorithm starts by dividing the molecule into vibrating subunits. The atoms in these subunits are connected by chemical bonds and for the normal mode of interest have contributions to the EDTM that point in a similar direction, that is, they add up constructively. The optimal coupling fragments are subsequently determined by systematically adding and removing subunits to the two coupling fragments. The best fragments are selected by maximizing an heuristic function $Q^{\mathbf{GCO}}(j)$ given by

$$Q^{\mathbf{GCO}}(j) = 0.3^{Nl} * 0.6^{Nc-2} * \frac{|R_{01}^{\mathbf{GCO}}(j)|}{0.75|R_{01}^{\mathbf{IF}}(j)| + |R_{01}^{\mathbf{R}}(j)|} \quad (8)$$

where $Q^{\mathbf{GCO}}$ is the "quality" of the coupling fragments, *Nl* the number of atoms part of the coupling fragments but not bound to other atoms in the fragment, and *Nc* is the number of atom clusters that are part of the two coupling fragments. The aim of the GCO analysis is to find fragments such that their coupling dominates the VCD signal. $Q^{\mathbf{GCO}}$, therefore, is chosen such that it increases with the size of the $R_{01}^{\mathbf{GCO}}(j)$ coupling, while it decreases for increasing values of the $R_{01}^{\mathbf{IF}}(j)$ and $R_{01}^{\mathbf{R}}$ contributions. Since $R_{01}^{\mathbf{IF}}(j)$ is still coming from the fragments that are taken into account it is multiplied by 0.75 to slightly reduce the penalty. In the definition of $Q^{\mathbf{GCO}}$, there is a large penalty for *Nl*. This is because vibrations always require participation of two neighboring atoms and it is not logical to assign these two atoms to different coupling fragments. Also, there is a, albeit smaller, penalty for increasing *Nc*. The rationale behind this is to avoid the addition of lesser-contributing groups in different parts of the molecule and thus keeping the interpretation of the resulting fragments much more straightforward.

It is key to notice that the two GCO fragments are often not uniquely defined since there are no restrictions on how to divide the relevant atoms among the two GCO fragments or on the number of atoms that a GCO fragment should contain.

DOI: 10.1021/acs.jcim.9b00956
J. Chem. Inf. Model. 2020, 60, 259−267

For example, when analyzing delocalized modes in larger molecules, one often encounters situations in which the two GCO fragments are physically not well separated and some of the atoms can be assigned either to fragment **A** or to fragment **B** without changing significantly the value computed for the Q^{GCO}. Since the goal of the GCO analysis is to provide physical insight into the origin of the VCD signal, the general rule of thumb in situations like this is to define GCO fragments that provide the best physical or chemical insight into the studied situation (and ignore any small variations observed in the Q^{GCO} values). Indeed, as will be illustrated in the Applications section, a careful consideration of the GCO fragments is crucial for a correct interpretation of the VCD spectra.

Computing Local Normal Mode Contributions. A final main feature of VCDtools is that it allows its user to compute the normal mode contributions of selected regions. Since this can be done for all normal modes at the same time, this is a quick method to identify specific modes in the spectrum. This is especially useful for large molecules with a plethora of normal modes containing mixtures of vibrations. By performing the normal mode localization analysis for multiple groups at the same time, information can also be obtained regarding the groups that vibrate together in each normal mode.

Applications. VCDtools is useful for a broad range of applications. In VCD spectroscopy it is not always the case that a good agreement between theory and experiment is obtained by following a standard protocol. The main reason for this is the high sensitivity of the technique to details of the molecular structure. The $R_{01}^{GCO}(j)$ term is often the dominant source of the VCD signal and its contribution highly depends on both the extent of the vibrational coupling and the relative orientation of the groups that are coupled. Being able to identify this coupling contribution therefore is crucial for recognizing—and dealing with—how issues such as large-amplitude motions, implicit solvent effects, incorrect local energy minima, or the use of an unsuitable level of theory ultimately affect the calculated VCD spectrum of the system of interest. In the following we will demonstrate this using three examples where we have used VCDtools to elucidate and resolve problems with computed VCD spectra, even to such an extent as to prevent the assignment of a spectrum to the incorrect enantiomer.

Identifying Problems with Large-Amplitude Motion. As a first application example, we consider 3-methyl-1-(methyldiphenlsilyl)-1-phenylbutan-1-ol, or in short silyl-alcohol (see Figure 2a). Our VCD studies on this molecule showed that there is a good overlap between theory and experiment except for the 1160−1380 cm^{-1} region, where the calculated spectra featured VCD bands with a large intensity that were absent in the experiment.[28] A thorough GCO analysis of the VCD bands in this region has revealed that this mismatch is caused by the large-amplitude motions of the OH-group, which are not simulated properly (see Figure 2b). Interestingly, to our surprise the difference between theory and experiment was not due to the rotation of the OH group like we had found before for a different system[24] but to the much more restricted OH-bending motion. In this section, we explain using VCDtools what the underlying reason is for this surprising insensitivity to the OH-rotation and demonstrate how VCDtools can be used to identify such issues associated with large-amplitude motion.

In the following, we consider the lowest-energy conformer of silyl-alcohol and discuss its most intense band in the problematic frequency interval between 1160 and 1380 cm^{-1}. The nuclear displacement vectors represented by the white arrows in Figure 2a show that this normal mode is a combination of CH and OH bending modes. By scaling the atom spheres according to the magnitudes of the atomic EDTMs we identify the OH bond and also the phenyl and isobutyl groups that are attached to the chiral center as the main sources of EDTM in this mode. The GCO analysis shows that the intense VCD signal computed for this mode is caused by the through-space interaction between the OH bond and the phenyl and isobutyl groups: $R_{01}^{GCO} = +64$, $R_{01}^{IF} = -9$, and $R_{01}^{R} = +0.5 \times 10^{-44}$ esu^2 cm^2. Importantly, the normal-mode analysis performed in Table 1 shows that the OH-bending vibration is delocalized over the entire problematic region. After performing GCO analyses on the more intense bands, it was concluded that the coupling of the OH and CH bending motions is indeed the fundamental reason for the mismatch between theory and experiment.[28]

Table 1. Rotational Strengths and Normal Mode Localizations of the Modes in the Problematic Region between 1160 and 1380 cm^{-1} for the Lowest-Energy Conformer of Silyl-Alcohol[a]

frequency	R_{01}	fragment A	fragment B
1150	+0.0	0.1	1.4
1155	−20.2	7.1	90.0
1173	−5.5	5.9	86.0
1177	−0.5	0.4	2.2
1181	+3.0	0.3	6.8
1220	−6.2	13.2	81.7
1241	+10.7	0.4	5.1
1275	−14.4	1.3	89.3
1283	+5.9	0.4	9.9
1289	−3.7	0.5	7.2
1296	−3.5	8.2	87.4
1318	−2.1	12.3	79.2
1325	−21.3	2.8	65.7
1326	+7.0	0.8	28.8
1329	−9.5	1.6	29.2
1334	+3.3	1.7	87.1
1340	+ 54.8	16.4	75.8
1352	+1.8	2.5	95.4

[a]Fragment A is the OH group, while fragment B encompasses the phenyl and isobutyl group (see Figure 2a in main text). The frequency is given in cm^{-1}, the rotational strength in 10^{-44} esu^2 cm^2, and the normal mode contributions in %.

An important observation is that the extent to which atoms contribute to the normal mode is only weakly linked to their contribution to the VCD signal. The OH-bending contribution to the normal modes is completely smeared out over the 1160−1380 cm^{-1} region with a maximum of 16% contribution at the most intense peak. Still, it is this contribution that, via the GCO mechanism, dominantly contributes to the VCD signals in this region, which, at a more fundamental level, is because polar bonds displace more charge thereby producing larger DTMs.

From this insight into the source of the signal, it was straightforward to conclude that the orientation of the OH group was crucial for the VCD signal in the region that was not computed correctly. A first attempt to take the rotation of the OH group into account did, however, hardly change the

DOI: 10.1021/acs.jcim.9b00956
J. Chem. Inf. Model. 2020, 60, 259−267

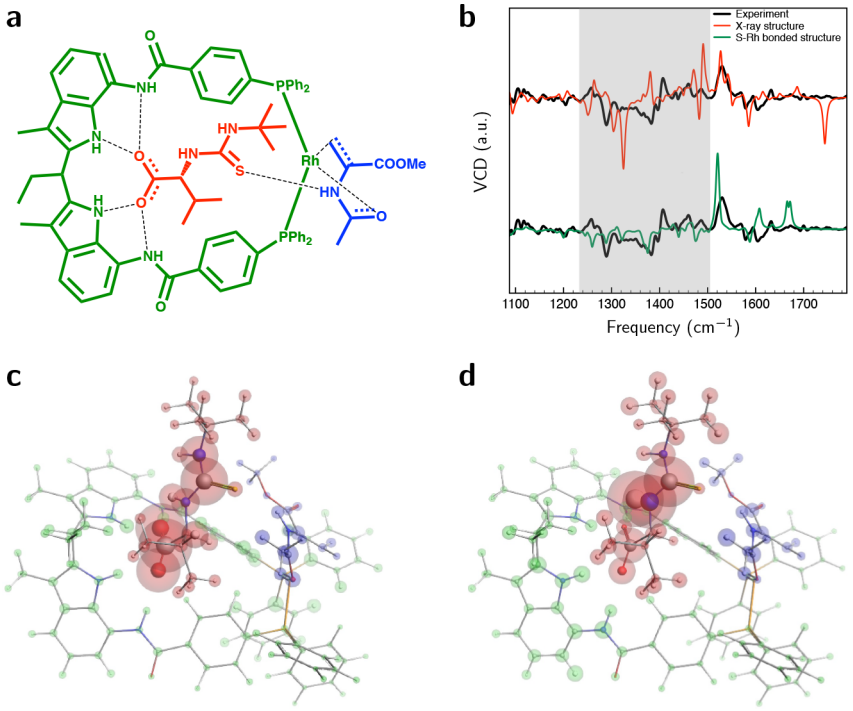

Figure 3. (a) Schematic representation of the catalyst complex with the catalyst in green, the cofactor in red and the substrate in blue. (b) Experimental and computed VCD spectra of the catalyst complex. Top panel: Comparison with the computed spectrum of the X-ray structure. Bottom panel: comparison with the spectrum computed for the S−Rh bonded structure. Panels c and d display the structure of the catalyst complex with the atomic spheres scaled with their atomic EDTM contributions to modes at 1299 and 1462 cm^{-1}, respectively.

spectrum.[28] The VCDtools option that was subsequently developed and that directly showed the EDTM and MDTM vectors of the coupling fragments inside the molecule quickly allowed for understanding this result. From the GCO analysis discussed above, it is known that nearly all of the R_{01}^{GCO} contribution comes from the interaction of the EDTM of the OH group and the MDTM of the phenyl and isobutyl groups. From Figure 2b, it becomes clear that the direction of the EDTM of the OH group is perpendicular to the bond. Rotating the OH group thus has little effect on the orientation of this vector with respect to the rest of the molecule and the VCD signal thus indeed is expected to change only slightly under such motions. The bending of the OH group on the other hand directly changes the angles, which is one of the reasons why it had such a large effect on the VCD spectrum.[28]

Investigating Structures of Molecular Complexes. The added value of the VCDtools implementation becomes even more clear when studies of larger molecular systems are considered. As second example, we, therefore, use a large metal−organic catalyst that forms a noncovalently bound complex with a cofactor and a substrate (see Figure 3a).[16] Depending slightly on the cofactor that is used the resulting complex contains about 170 atoms and, thus, has over 500 normal modes. Because of the size and complexity of the system it is not feasible to perform a conventional conformational search. Instead, we, therefore, started on a structure based on the crystal structure found by X-ray spectroscopy.

Figure 3b shows the experimentally recorded spectrum and the spectrum calculated based on the X-ray structure (for the experimental and computational details see refs 16 and 17). As can be seen, the match between experiment and calculation is rather poor and definitely much poorer than what one nowadays can expect. Especially in the region between 1240 and 1500 cm^{-1}, there are many intense bands in the calculation that are absent in the experiment. Using the atom scaling function in VCDtools allowed us to quickly scan the intense bands in that region which showed that most of the signal arises from the cofactor. As examples, in Figure 3c and 3d, two modes are shown that correspond to the most intense VCD bands at 1300 and 1462 cm^{-1}. Using the VCDtools option to scale the atomic spheres by their atomic EDTM contribution clearly highlights the cofactor in that region. A GCO analysis with the cofactor in one fragment and the rest of the complex in the other fragment confirms that almost all of the intense signals in the 1240−1500 cm^{-1} region are either from the cofactor itself or from the interaction between the cofactor and the other two parts of the molecular complex (see Table 2).

The observation that these bands are calculated incorrectly, therefore, strongly suggests that the cofactor is not bound properly to the complex in the employed structure and that its structure needs to be adjusted significantly. This prompted us to rearrange the thioureum group of the cofactor to form an additional hydrogen bond with the substrate. During the DFT geometry optimization the structure converged further to form an intermolecular interaction between the sulfur atom of the cofactor and the rhodium atom of the catalyst. The energy of the final structure that was obtained was found to be significantly lower than that of the initially employed X-ray structure, but more importantly, a much better match of the calculated VCD spectrum with the experiment was obtained as can be concluded from Figure 3b. The interaction between the rhodium and sulfur atoms was afterward indeed confirmed by means of NMR.[17]

Resolving Incorrectly Computed VCD Signs. A final example that will be discussed is a rotaxane that we are currently investigating with VCD and that is depicted in Figure

DOI: 10.1021/acs.jcim.9b00956
J. Chem. Inf. Model. 2020, 60, 259−267

Table 2. Rotational Strengths and Its Decomposition for the Intense ($R_{01} \geq 100$) VCD Modes in the Problematic Region between 1240 and 1500 cm^{-1} of the Catalyst Complex (See Figure 3)[a]

frequency	R_{01}	$R_{01}^{IF,A}$	R_{01}^{GCO}
1278	−187	−48	−119
1298	−100	−25	−60
1299	**−383**	**−375**	**+0**
1354	+221	+ 114	+112
1360	−109	−2	−10
1442	+117	−10	+69
1485	−167	+7	−62
1455	−192	+21	−121
1459	+117	+79	+31
1462	**+351**	**+195**	**+139**

[a]Fragment **A** is the cofactor, and fragment **B** is the rest of the molecule, $R_{01}^{IF,A}$ is the R_{01}^{IF} of Fragment **A** only, and R_{01}^{GCO} is the signal arising from the coupling between fragments **A** and **B**. The frequency is given in cm^{-1}, and the rotational strengths are in 10^{-44} esu^2 cm^2.

4a. These rotaxanes consist of two mechanically interlocked parts, a thread and a macrocycle. From a chirality point of view, the structure is highly interesting as it displays two types of chirality. First, there is a point chirality in the thread but there is also a second chiral element in the form of the mechanically planar (MP) chirality that arises from the orientation of the asymmetric macrocyle on the thread. These rotaxanes can be synthesized stereoselectively, which allows for the study of enantiopure samples whose chirality was previously determined by X-ray diffraction.[47] Here, we will only discuss the VCD of the (R,R_{mp})-**4** rotaxane where the first "R" corresponds to the point chirality of the thread, the "R_{mp}" to the mechanically planar chirality of the complex, and the label "**4**" was taken as the label for the rotaxane as is used in Jinks et al.[47]

The experimentally recorded and theoretically predicted VCD spectrum of (R,R_{mp})-**4** are shown in Figure 4b. Initially, we calculated the geometries, energies and spectra using a dispersion correction.[48] As the macrocycle and thread of the rotaxane are held in place by medium-long-range interactions one would expect that this dispersion term—which is important in this range—would lead to an improved prediction of conformational structures. Surprisingly, however, the comparison of experimental and computed spectra shows that many key VCD bands highlighted in Figure 4 show opposite signs. The fact that the experimental VCD spectrum of rotaxane (R_{mp})-**5**, which is similar to (R,R_{mp})-**4**,[47] was correctly reproduced by calculations, suggested that the experimental (R,R_{mp})-**4** results might not have been correct. However, as will be shown below a careful analysis of the modes that exhibited opposite VCD signs using VCDtools reveals that the observed discrepancies between theory and experiment result from the uncertainties associated with level of theory used in calculations.

In Figure 4c, the structure of rotaxane (R,R_{mp})-**4** is shown with the atomic spheres scaled to the EDTMs of the normal mode at 1450 cm^{-1}, which has a large VCD signal with an opposite sign. As can be seen, most of the VCD intensity arises from the ring. The GCO analysis on this mode leads to the conclusion that the coupling between the two halves of the ring (see Figure 4) is responsible for most of the VCD signal

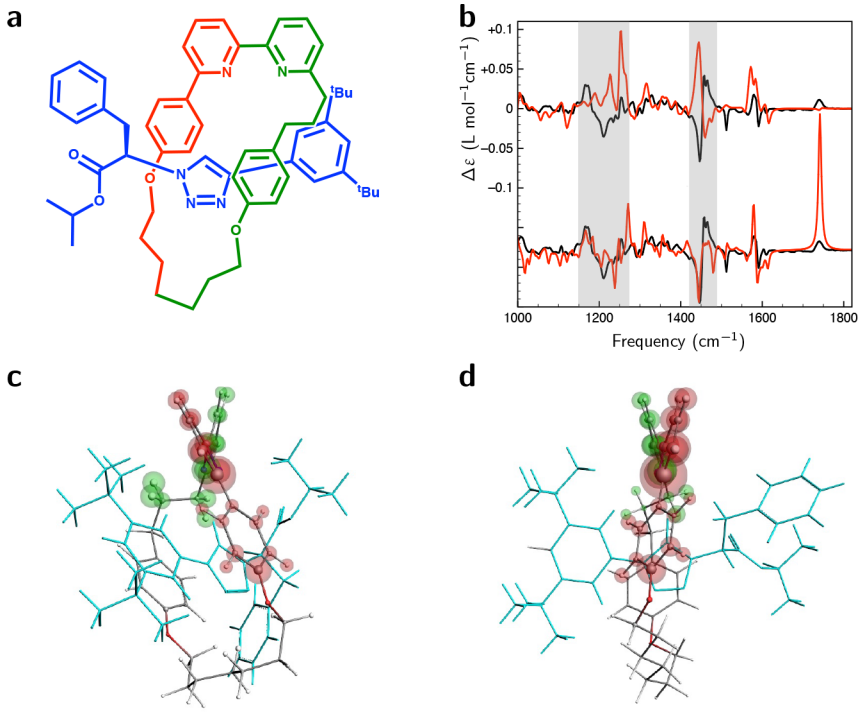

Figure 4. (a) Schematic representation of the (R,R_{mp})-**4** rotaxane with the thread in blue and the macrocycle in red and green. (b) Experimental (black) and computed VCD spectra (red). Top panel: Comparison with spectrum computed using dispersion correction. Bottom panel: Comparison with the computed spectrum computed without dispersion correction. Lowest-energy structures calculated with and without the dispersion term are displayed in panels c and d, respectively. The atomic spheres are scaled for the atomic EDTMs of the normal mode at 1450 cm^{-1}, which has a large VCD intensity. The interacting fragments are highlighted in red and green. For visibility the thread is colored light blue and represented as a stick structure.

DOI: 10.1021/acs.jcim.9b00956
J. Chem. Inf. Model. 2020, 60, 259−267

(+90 out of +139 × 10^{-44} esu^2 cm^2). A GCO analysis of the other incorrectly computed VCD signals shows that also there the coupling with or within the ring plays an important role. The structure of the ring thus clearly is a key factor. Upon analysis of the structures and comparing them with the low-energy structures found for (R_{mp})-**5**, we noticed that the angle between the two pyridine groups at the top of the ring in Figure 4 was different. For (R,R_{mp})-**4**, the dihedral angle of the N−C−C−N group in the bipyridine is +40°, while in the (R_{mp})-**5** structure, this angle is −35°. Overall, this implies that the axial chirality of the bipyridine is changed in the two structures, and thereby for a large part of the ring as well.

Since this axial chirality of the bipyridine group is not enforced by any strong molecular interactions, both *P* and *M* forms are present within the 600+ conformations found for the rotaxanes. When using the dispersion correction term in the geometry optimization calculations the structures with the incorrect *P* axial chirality apparently are preferred for (R,R_{mp})-**4**. Without the dispersion term, on the other hand, all the calculated energies change drastically. Now the structures with the *M* axial chirality are the lowest ones in energy resulting in a predicted VCD spectrum that is in nice agreement with the experimental one. (see bottom spectra in Figure 4b). As an example, Figure 4d shows the lowest-energy structure. Performing a GCO analysis on the intense VCD band at 1450 cm^{-1} reveals that the coupling is now indeed reversed in sign (−92 out of −116 × 10^{-44} esu^2 cm^2).

This example demonstrates another important aspect of the analysis using the GCO approach. The GCO mechanism indeed leads to large signals that are observable in the experiment but those signals are extremely sensitive to the orientation of the coupling groups. It is, therefore, quite important to check the main bands of a measured spectrum and determine the origin of the VCD signal. When these signals are mainly coming from the coupling between two fragments, one needs to be cautious that the correct low-energy structures are being found in the calculations. In the present case, the stereochemistry of the studied rotaxane would have been assigned incorrectly as the main features of the experimental spectrum were incorrectly predicted by the initial calculations. Beforehand, it could not have been expected that using the dispersion correction term would change the axial chirality of a particular group in the ring which also happens to be one of the main sources of intensity in the VCD spectrum. It is only via a careful analysis, as made possible by VCDtools, that one is able to recognize the weak points in the assignment and to understand the key elements responsible for the appearance of the spectrum. VCDtools, thus, is an indispensable tool for furthering our understanding and assignment of VCD spectra.

CONCLUSIONS AND OUTLOOK

We have introduced and described the implementation of the VCDtools program into the ADF GUI. This program allows for a much quicker and in-depth analysis of computed VCD spectra and provides visualization aides that ease such an analysis, especially for large molecules or molecular complexes. In the three application examples we demonstrated the importance of the GCO mechanism for interpreting a VCD spectrum. The mechanism directly explains the origin of the dominant VCD spectral features but also shows why and how these features are sensitive to particular contributions from normal modes and orientation of the fragments that are coupled. Because of this sensitivity small errors in the computation can have major effects on the computed VCD spectrum. It has been shown that using VCDtools it is quite straightforward to determine which part of the molecule is computed incorrectly, giving crucial hints to solve problems in the comparison between experiment and calculation. This provides extensive insight about what causes differences between theory and experiment and in the end often leads to a better agreement between the two.

The three examples discussed here might seem extreme cases as in literature computed VCD spectra are rarely reported to have such large differences with the experiment. This is to a large extent due the positive results bias in the publication process. Right now it is estimated that about 20% of the molecules investigated with VCD show large differences between theory and experiment. Moreover, because of the increase in the amount and accessibility of computational resources, more complex molecular structures will be investigated with VCD, which are more prone to have problems associated with their calculations. This implementation of VCDtools provides an essential means to understand and resolve these issues and prevent incorrect assignments of the stereochemistry and conformational distributions of such systems.

AUTHOR INFORMATION

Corresponding Authors

*E-mail: w.j.buma@uva.nl.
*E-mail: vp.nicu@gmail.com.

ORCID

Lucas Visscher: 0000-0002-7748-6243
Wybren J. Buma: 0000-0002-1265-8016

Notes

The authors declare no competing financial interest.

ACKNOWLEDGMENTS

M.A.J.K., L.V., and W.J.B. acknowledge financial support from NWO in the framework of the Fund New Chemical Innovations (NWO Project No. 731.014.209). V.P.N. acknowledges funding from UEFISCDI (PN-III-P1-1.1-TE-2016-1049, contract no. 46/2018). We furthermore acknowledge useful discussions with Dr. Stan van Gisbergen from S.C.M.

REFERENCES

(1) Berova, N.; Polavarapu, P. L.; Nakanishi, K.; Woody, R. W. *Comprehensive Chiroptical Spectrosocopy*, Vol. *1*−*2*; John Wiley & Sons: New York, NY, 2012.

(2) Nafie, L. A. *Vibrational Optical Activity*, 1st ed.; John Wiley & Sons, 2011.

(3) Stephens, P. J.; Devlin, F. J.; Cheeseman, J. R. *VCD Spectroscopy for Organic Chemists*; CRC Press, 2012.

(4) Polavarapu, P. L. *Chiroptical Spectroscopy: Fundamentals and Applications*, 1st ed.; CRC Press: Boca Raton, 2016.

(5) Chamayou, A. C.; Lüdeke, S.; Brecht, V.; Freedman, T. B.; Nafie, L. A.; Janiak, C. Chirality and Diastereoselection of Δ/Λ-Configured Tetrahedral Zinc Complexes Through Enantiopure Schiff Base Complexes: Combined Vibrational Circular Dichroism, Density Functional Theory, 1H NMR, and X-ray Structural Studies. *Inorg. Chem.* **2011**, *50*, 11363−11374.

(6) Merten, C.; Pollok, C. H.; Liao, S.; List, B. Stereochemical Communication Within a Chiral Ion Pair Catalyst. *Angew. Chem., Int. Ed.* **2015**, *54*, 8841−8845.

DOI: 10.1021/acs.jcim.9b00956
J. Chem. Inf. Model. 2020, 60, 259−267

(7) Batista, J. M., Jr.; Blanch, E. W.; da Silva Bolzani, V. Recent Advances in the Use of Vibrational Chiroptical Spectroscopic Methods for Stereochemical Characterization of Natural Products. *Nat. Prod. Rep.* **2015**, *32*, 1280−1302.
(8) Ma, S.; Cao, X.; Mak, M.; Sadik, A.; Walkner, C.; Freedman, T. B.; Lednev, I. K.; Dukor, R. K.; Nafie, L. A. Vibrational Circular Dichroism Shows Unusual Sensitivity to Protein Fibril Formation and Development in Solution. *J. Am. Chem. Soc.* **2007**, *129*, 12364−12365.
(9) Dzwolak, W. Chirality and Chiroptical Properties of Amyloid Fibrils. *Chirality* **2014**, *26*, 580−587.
(10) Kurouski, D. Advances of Vibrational Circular Dichroism (VCD) in Bioanalytical Chemistry. A Review. *Anal. Chim. Acta* **2017**, *990*, 54−66.
(11) Schwartz, E.; Domingos, S. R.; Vdovin, A.; Koepf, M.; Buma, W. J.; Cornelissen, J. J. L. M.; Rowan, A. E.; Nolte, R. J. M.; Woutersen, S. Direct Access to Polyisocyanide Screw Sense Using Vibrational Circular Dichroism. *Macromolecules* **2010**, *43*, 7931−7935.
(12) Sato, H.; Yajima, T.; Yamagishi, A. Chiroptical Studies on Supramolecular Chirality of Molecular Aggregates. *Chirality* **2015**, *27*, 659−666.
(13) Kim, T.; Mori, T.; Aida, T.; Miyajima, D. Dynamic Propeller Conformation for the Unprecedentedly High Degree of Chiral Amplification of Supramolecular Helices. *Chem. Sci.* **2016**, *7*, 6689−6694.
(14) Moulin, E.; Armao, J. J., IV; Giuseppone, N. Triarylamine-Based Supramolecular Polymers: Structures, Dynamics, and Functions. *Acc. Chem. Res.* **2019**, *52*, 975−983.
(15) Osypenko, A.; Moulin, E.; Gavat, O.; Fuks, G.; Maaloum, M.; Koenis, M. A. J.; Buma, W. J.; Giuseppone, N. Temperature Controlled Hierarchical Supramolecular Polymerization of Chiral Triarylamines. *Chem. - Eur. J.* **2019**, *25*, 13008−13016.
(16) Strudwick, B. H. Bringing to Light Transient Molecular Structure and Function Using Advanced Vibrational Spectroscopy. Ph.D. thesis, University of Amsterdam, 2019.
(17) Bai, S. Supramolecular Transition Metal Catalysis: Effector Controlled Catalysis and Supramolecular Substrate Preorganization. Ph.D. thesis, University of Amsterdam, 2019.
(18) Fedorovsky, M. Exploring Vibrational Optical Activity with PyVib2. *Comput. Lett.* **2006**, *2*, 233−236.
(19) Zerara, M. PyVib, a Computer Program for the Analysis of Infrared and Raman Optical Activity. *J. Comput. Chem.* **2008**, *29*, 306−311.
(20) Hug, W.; Fedorovsky, M. Characterizing Vibrational Motion Beyond Internal Coordinates. *Theor. Chem. Acc.* **2008**, *119*, 113−131.
(21) Liégeois, V.; Champagne, B. Implementation in the Pyvib2 Program of the Localized Mode Method and Application to a Helicene. *Theor. Chem. Acc.* **2012**, *131*, 1284.
(22) Nicu, V. P.; Baerends, E. J.; Polavarapu, P. L. Understanding Solvent Effects in Vibrational Circular Dichroism Spectra: [1,1′-Binaphthalene]-2,2′-diol in Dichloromethane, Acetonitrile, and Dimethyl Sulfoxide Solvents. *J. Phys. Chem. A* **2012**, *116*, 8366−8373.
(23) Heshmat, M.; Baerends, E. J.; Polavarapu, P. L.; Nicu, V. P. The Importance of Large-Amplitude Motions for the Interpretation of Mid-Infrared Vibrational Absorption and Circular Dichroism Spectra: 6,6′-Dibromo-[1,1′-binaphthalene]-2,2′-diol in Dimethyl Sulfoxide. *J. Phys. Chem. A* **2014**, *118*, 4766−4777.
(24) Nicu, V. P.; Domingos, S. R.; Strudwick, B. H.; Brouwer, A. M.; Buma, W. J. Interplay of Exciton Coupling and Large-Amplitude Motions in the Vibrational Circular Dichroism Spectrum of Dehydroquinidine. *Chem. - Eur. J.* **2016**, *22*, 704−715.
(25) Polavarapu, P. L. Determination of the Absolute Configurations of Chiral Drugs Using Chiroptical spectroscopy. *Molecules* **2016**, *21*, 1056.
(26) Kreienborg, N. M.; Pollok, C. H.; Merten, C. Towards an Observation of Active Conformations in Asymmetric Catalysis: Interaction-Induced Conformational Preferences of a Chiral Thiourea Model Compound. *Chem. - Eur. J.* **2016**, *22*, 12455−12463.
(27) Merten, C. Vibrational Optical Activity as Probe for Intermolecular Interactions. *Phys. Chem. Chem. Phys.* **2017**, *19*, 18803−18812.
(28) Xia, Y.; Koenis, M. A. J.; Collados, J. F.; Ortiz, P.; Harutyunyan, S. R.; Visscher, L.; Buma, W. J.; Nicu, V. P. Regional Susceptibility in VCD Spectra to Dynamic Molecular Motions: The Case of a Benzyl α-Hydroxysilane. *ChemPhysChem* **2018**, *19*, 561−565.
(29) Johnson, J. L.; Polavarapu, P. L. Chiral Molecular Structures of Substituted Indans: Ring Puckering, Rotatable Substituents, and Vibrational Circular Dichroism. *ACS Omega* **2019**, *4*, 4963−4976.
(30) Nicu, V. P. Revisiting an Old Concept: the Coupled Oscillator Model for VCD. Part 1: The Generalised Coupled Oscillators Mechanism and its Intrinsic Connection to the Strength of VCD Signals. *Phys. Chem. Chem. Phys.* **2016**, *18*, 21202−21212.
(31) Holzwarth, G.; Chabay, I. Optical Activity of Vibrational Transitions: A Coupled Oscillator Mode. *J. Chem. Phys.* **1972**, *57*, 1632−1635.
(32) Stephens, P. J. Gauge Dependence of Magnetic Dipole Transition Moments and Rotational Strength. *J. Phys. Chem.* **1987**, *91*, 1712−1715.
(33) Bour, P.; Keiderling, T. A. Computational Evaluation of the Coupled Oscillator Model in the Vibrational Circular Dichroism of Selected Small Molecules. *J. Am. Chem. Soc.* **1992**, *114*, 9100−9105.
(34) Covington, C. L.; Nicu, V. P.; Polavarapu, P. L. Determination of the Absolute Configurations Using Exciton Chirality Method for Vibrational Circular Dichroism: Right Answers for the Wrong Reasons? *J. Phys. Chem. A* **2015**, *119*, 10589−10601.
(35) Abbate, S.; Bruhn, T.; Pescitelli, G.; Longhi, G. Vibrational Optical Activity of BODIPY Dimers: The Role of Magnetic-Electric Coupling in Vibrational Excitons. *J. Phys. Chem. A* **2017**, *121*, 394−400.
(36) Dalton program suite. http://daltonprogram.org.
(37) Amsterdam Density Functional program. http://www.scm.com.
(38) Gaussian 16. http://www.gaussian.com.
(39) PQS Software. http://www.pqs-chem.com.
(40) Furche, F.; Ahlrichs, R.; Hättig, C.; Klopper, W.; Sierka, M.; Weigend, F. Turbomole. *Wiley Interdiscip. Rev.: Comput. Mol. Sci.* **2014**, *4*, 91−100.
(41) Nicu, V. P. Revisiting an Old Concept: the Coupled Oscillator Model for VCD. Part 2: Implications of the Generalised Coupled Oscillator Mechanism for the VCD Robustness Concept. *Phys. Chem. Chem. Phys.* **2016**, *18*, 21213−21225.
(42) Nicu, V. P.; Neugebauer, J.; Baerends, E. J. Effects of Complex Formation on Vibrational Circular Dichroism Spectra. *J. Phys. Chem. A* **2008**, *112*, 6978−6991.
(43) Nicu, V. P.; Autschbach, J.; Baerends, E. J. Enhancement of IR and VCD intensities due to charge transfer. *Phys. Chem. Chem. Phys.* **2009**, *11*, 1526−1538.
(44) Rosenfeld, L. Quantenmechanische Theorie der natürlichen optischen Aktivität von Flüssigkeiten und Gasen. *Eur. Phys. J. A* **1929**, *52*, 161−174.
(45) Stephens, P. J. Theory of Vibrational Circular Dichroism. *J. Phys. Chem.* **1985**, *89*, 748−752.
(46) Fonseca Guerra, C.; Snijders, J. G.; te Velde, G.; Baerends, E. J. Towards an Order-N DFT Method. *Theor. Chem. Acc.* **1998**, *99*, 391−403.
(47) Jinks, M. A.; de Juan, A.; Denis, M.; Fletcher, C. J.; Galli, M.; Jamieson, E. M.; Modicom, F.; Zhang, Z.; Goldup, S. M. Stereoselective Synthesis of Mechanically Planar Chiral Rotaxanes. *Angew. Chem., Int. Ed.* **2018**, *57*, 14806−14810.
(48) Grimme, S.; Ehrlich, S.; Goerigk, L. Effect of the Damping Function in Dispersion Corrected Density Functional Theory. *J. Comput. Chem.* **2011**, *32*, 1456−1465.

DOI: 10.1021/acs.jcim.9b00956
J. Chem. Inf. Model. 2020, 60, 259−267